Proceedings of the 12th International Conference on
Aluminium Alloys, September 5-9, 2010, Yokohama, Japan

pp. 2369-2374

Analysis of Crack-Tip Field via Observation of Local Crack Extension by Means of Fast Tomography Technique

Shohei Yamauchi[1], Hiroyuki Toda[1], Masakazu Kobayashi[1], Takashi Hiramatsu[1], Eric Maire[2]

[1]Department of Mechanical Engineering, Toyohashi University of Technology, Toyohashi, Aichi, Japan

[2]GEMPPM UMR, CNRS, Campus Gérard Mégie, rue Michel-Ange, 16[e] arrondissement de Paris, France

A high-time-resolution 3D imaging has been performed to observe crack propagation behaviors through an aluminum alloy. The experiment was carried out at a white X-ray beamline in Europian Synchrotron Radiation Facility (ESRF). This high speed imaging requiring only 22.5 sec has been achieved to investigate the in-situ fracture characteristics without interrupting at a reasonable spatial resolution level (4.1μm). It has been clarified that the complex local crack extension behaviors are significantly affected due to the existence of dispersed particles and hydrogen micro pores. The comparison of crack-tip strain field with an asymptotic solution for the elastic-plastic fracture has revealed the transition in crack-tip stress singularity from the HRR field for stationary cracks to the RDS field for the propagating cracks when crack propagation is observed. It has been identified that the current technique can provide a unique possibility to assess such dynamic phenomena.

Keywords: *High-resolution X-ray tomography, Fracture mechanics, Crack propagation, HRR field, RDS field*

1. Introduction

Analysis of crack extension allows the fracture assessment of structure materials because it accompanies crack growth. In our previous study, the in-situ observation of crack extension has been visualized with the ordinary high-resolution X-ray tomography technique[1-3]. It is the only way to get three dimensional images of a crack propagation and growth in some load steps. However, we had to interrupt the test, resulting in significant stress relaxation during scanning, because about 20 to 60 minutes were necessary for scanning. The application of *J*-integral might not be validated due to the unloading process caused by stress relaxation.

In the present study, therefore, a fast tomography technique[4] with 22.5 sec scanning has been applied to visualize actual crack extension behaviors in a real in-situ manner. This technique, which can acquire the images with only one percent of the time needed for the traditional technique, has been used to observe the crack behavior. This study aims to investigate how and why the premature local crack extension occurs, and to analyze the crack-tip strain singular field with the data sets acquired by fast tomography technique.

2. Experimental Methods

2.1 Material and specimen preparation

The chemical compositions of the 2024-T361 aluminum alloy used in this work were given in Table 1.

Table 1 Chemical compositions of the 2024 alloy used in present study

(mass%)

Si	Fe	Cu	Mn	Mg	Cr	Zn	Ti	Al
0.04	0.11	4.41	0.62	1.57	<0.01	0.12	0.03	bal.

Conventional single-edge notched (SEN) specimens, 10 × 10 × 55 mm in size, were produced with a slit giving a ratio of an initial notch length *a*, to nominal width, *W* of 0.45. A fatigue pre-crack was then introduced into the specimen according to ASTM Standard E 647-95A until a/*W* (*a*, crack length) became about 0.37. Small parallelepiped specimens (shown in Fig. 1) were carefully machined from the crack-tip region of the fatigue pre-cracked SEN specimens using an electro-discharge machining so that *a*/*W* for the small parallelepiped specimen became about 0.5.

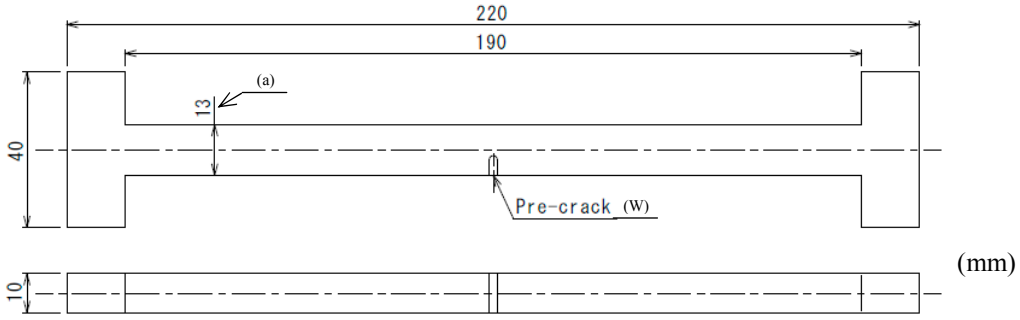

Fig. 1 Geometry of the tensile test specimen (*a*/*W*=0.5).

2.2 Tomographic imaging

The experiment was performed at ID15A beamline in ESRF (European Synchrotron Radiation Facility) in Grenoble, France. A white X-ray beam with photon energy of 60keV was used for the tomographic observation. X-ray micro-tomography setup consists of a high precision stage to position the sample in the X-ray beam, an in-situ tensile test rig on the stage and an imaging detector system to record images of the transmitted radiation. The detector consists of a CCD camera that has 1024×2048 pixel size and a scintillator of Lu3Al5O12:Eu. A load-displacement curve in the tensile test is shown in Fig. 2. The test was operated without interrupting and the speed was 2μm/s. Scanning was carried out thrice by traditional scanning system (slow CT) at early stages of the test and seven times by fast scanning system (fast CT) at later stages.

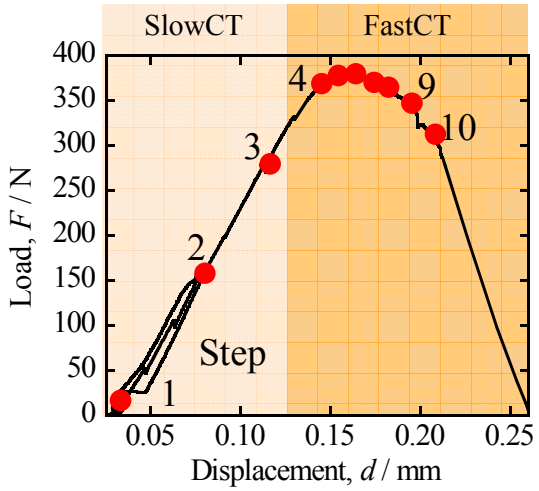

Fig. 2 Load-displacement curve in an in-situ tensile test. Tomographic scans were performed at representing loading steps.

2.3 Features of high-time-resolution 3D imaging

There are three main differences between present imaging and traditional imaging to achieve high graphical quality and fast shutter speed.

The first difference is type of X-ray. In present study, the white X-ray beam with energy tuned in 60keV was used. The white X-ray beam can take clear images of aluminum alloy, but the monochromatic X-ray beam does not have enough photon flux to obtain the images at a reasonable spatial resolution level.

The second one is read out speed and read time of CCD camera. The ordinary frame rate of CCD camera is 0.1frame/sec, but 60frame/s was acquired for the camera in the current experiment.

The last one is data acquisition architecture. Previous architecture operates to read out, save data, rotate specimen in order and the dead time is about 900ms. In this work, all of them were operated at the same time and the dead time is less than 1ms.

These changes allow the acquisition of CT images 100times faster than traditional CT.

3. Results and discussion

3.1 Assessment of the images

Resolution is the capability to separate two distinct objects that are located close to each other. Fig. 3 shows how to evaluate the spatial resolution of scanned images. At first, the boundary across the particle and aluminum interface was scanned, as indicated in Fig. 3 (a). Then the obtained profile in gray level was fitted with the sigmoid function and the full width at half maximum (FWHM) in its 1st derivation, 4.1μm in Fig. 3 (b), gave the quantitative spatial resolution.

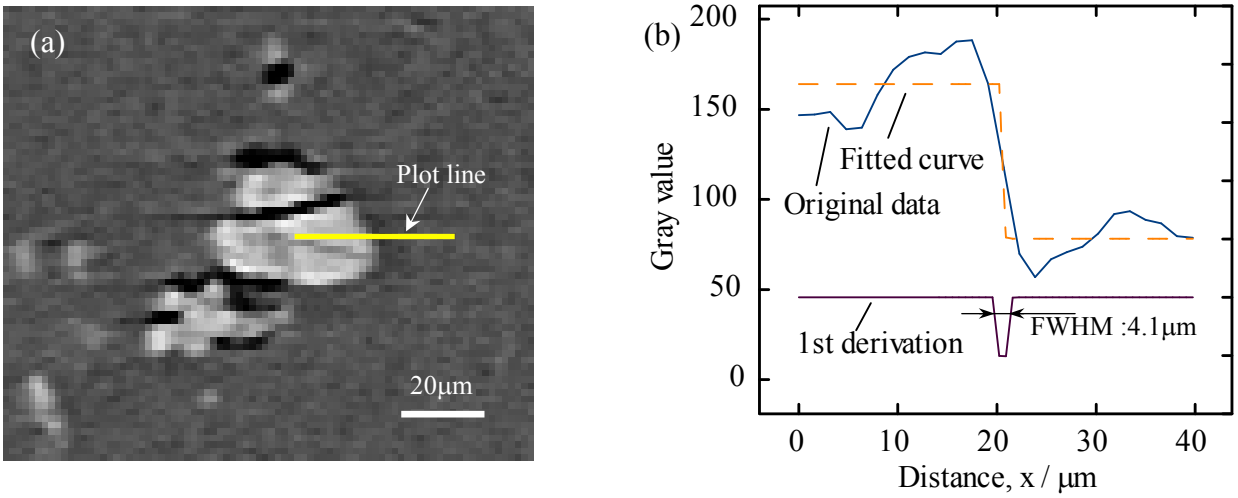

Fig. 3 Evaluation of spatial resolution at a particle/matrix interface shown in (a). (b) includes an original line profile across the interface the sigmoid fitting and its 1st derivation, resulting in a spatial resolution of about 4.1μm.

Fig. 4 shows virtual tomographic slice images acquired by both traditional tomography and fast tomography. The crack and some other microstructure features, such as dispared particles and micro pores, were observed clearly.

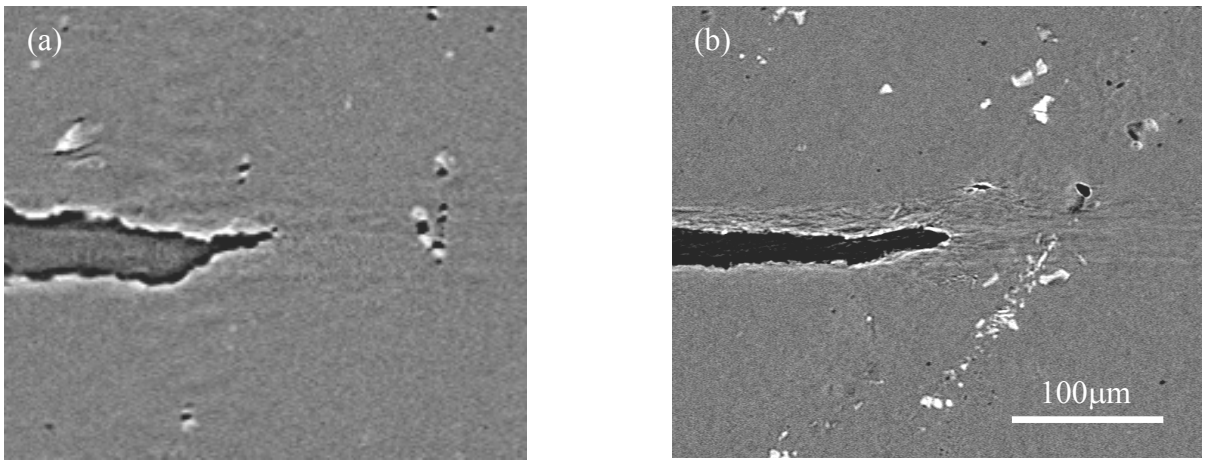

Fig. 4 Virtual tomographic slice images. (a) Fast tomographic technique; (b) Traditional tomographic technique.

For the fast tomography and traditional tomography, the spatial resolutions are 4.1μm and 1.0μm, respectively. And also the voxel sizes are 1.59μm and 0.497μm, respectively. When these two techniques are simply compared by the numerical value in spatial resolution or voxel size, fast tomography is inferior to traditional tomography. But the image quality in Fig. 4 (a) is clear enough to show the micro pores, particles and crack shape, leading to no influences to get images by technical problems.

3.2 Analysis of stress field

Interrelations between crack opening displacement δ(COD) and distance from crack-tip are defined by elastic-plastic fracture mechanics, as shown in equation (1) for Hutchenson - Rice - Rosengren (HRR) field at blunting crack and equation (2) for Rice – Drugan - Sham (RDS) field at growing crack.

$$\delta = 2\alpha'\varepsilon_0\left(\frac{J}{\alpha'\varepsilon_0\sigma_0 I_n}\right)^{n/(n+1)} r^{1/(n+1)}\tilde{u}(\pi) \tag{1}$$

$$\frac{E\delta}{\sigma_0 r} = \alpha T_R + \beta \ln\left(\frac{eR}{r}\right) \tag{2}$$

Where I_n and $u(\theta)$ are normalize functions, J is J-integral value, σ_0 is flow stress, E is Young's modulus, R is a size of plastic field and α, β, α', ε_0 are constant.

An example of COD profiles for all the loading steps is shown in Fig. 5. The COD is found to be increased as the load rises. It also shows that COD profiles near the crack-tip are becoming blunt at stationary crack, and becoming sharp at growing crack. These shapes of crack are theoretical shapes in each situation and these phenomena have not been observed by traditional tomographic technique.

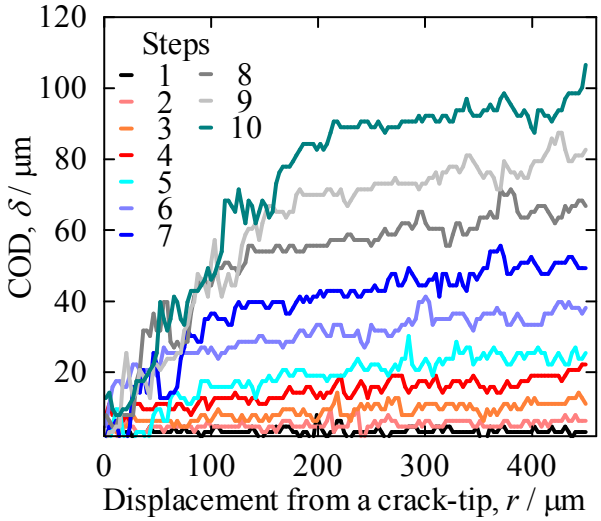

Fig. 5 COD crack profiles at 600μm in z direction for all loading steps.

The COD profiles were normalized by J-integral and the influences resulting from loading step and distance from crack-tip were removed[5]. Then the normalized COD profiles are shown in Fig. 6. A transition in stress singular field near the crack-tip is observed from HRR field to RDS field as the crack status changes from blunting to growing. And the stress singular field nearby the crack-tip fitting RDS field is becoming larger with the increasing load.

From the above observation, it is confirmed that the stress singular field near the crack-tip conforms to elastic-plastic fracture mechanics.

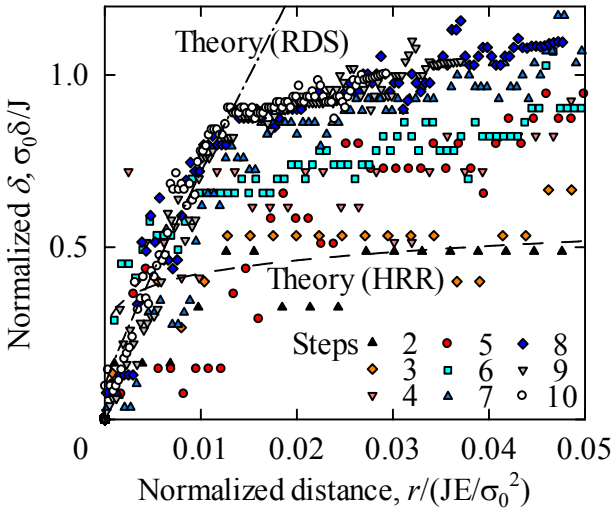

Fig. 6 Normalized crack opening profiles at 600μm in z direction for all loading steps.

3.3 Analysis of local crack propagation

The crack shape in vertical view and distribution of crack propagation in the specimen are complex, as shown in Fig. 7 (a), and those premature crack extensions are caused by the particles, micro pores and voids as shown in Fig. 7 (b). This phenomenon is caused by anti-shielding effect and the resulting load for the extension of premature crack is smaller than that for the general crack propagation.

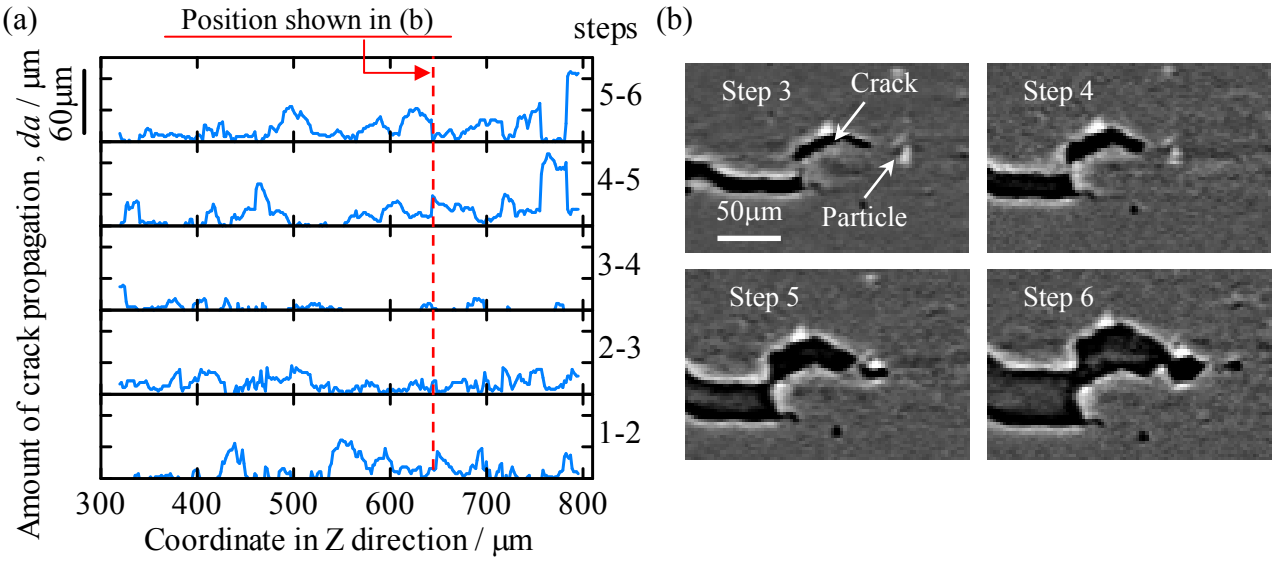

Fig. 7 Propagation of crack in the specimen. (a) variation in amount of crack propagation during slow crack growth; (b) virtual cross sections of local crack propagation behaviors at position indicated in (a).

On the other hand, it was analyzed that the stress singular field around crack-tip at step 5-6 which is on en route of transition of the field from HRR field to RDS field, and the result is shown in Fig.8. The areas with larger *da*, corresponding to the propagation of premature crack, conform to the RDS field, while the other areas having lower *da* follow the HRR field. An alternate transition is confirmed in the Z direction along the whole specimen.

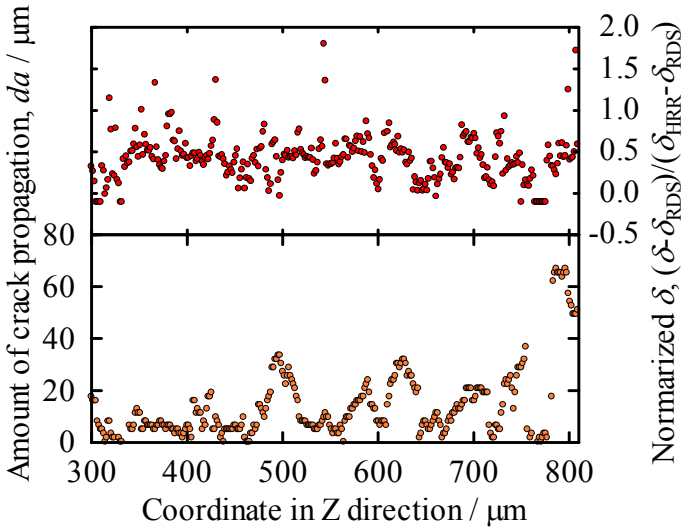

Fig. 8 Analysis of stress singular field around crack-tip at 5-6 loading step. Bottom figure shows amount of crack propagation. Top one shows normalized δ, in which the value 0 means the field fitting RDS and the value 1 means the field fitting HRR.

4. Conclusions

(1) A fast tomography has been used to observe the crack propagation behaviors during in-situ tensile test. The CT images acquired by the fast tomography are not affected by stress relaxation. And the crack, micro pores and particles can be identified in the images.
(2) Through analysis of the stress singular field around a crack-tip, it has been clarified that they are dominated by the HRR field at a blunting crack and also dominated by the growing crack singularity.
(3) Premature crack propagation is confirmed to be influenced by the existence of dispersed particles and hydrogen micro pores.
(4) Stress singular field around the position of premature crack extension shows a transition from the HRR singular to the RDS singular fields.

References

[1] H. Toda, J. –Y. Buffiere, E. Maire, K. H. Khor, P. Gregson and T. Kobayashi : Acta Mater. , 52 (2004) 1305-1317.
[2] H. Toda, S. Yamamoto, M. Kobayashi, K. Uesugi, H. Zhang : Acta Mater. , 56(2008) 6027-6039.
[3] H. Zhang, H. Toda, P. C. Qu, Y. Sakaguchi, M. Kobayashi, K. Uesugi, Y. Suzuki : Acta Mater. , 57(2009), 3287-3300
[4] M. D. Michiel, J. M. Merino, D. F. Carreiras, T. Muslaps, V. Honkimaki, P. Falus, T. Martins, O. Svensson: Review of Scientific Instruments. 76; 043702 (2005)
[5] K. S. CHAN : Metakk. Trans. A, 1990, vol.21A, pp.81-86